Energy Storage Materials 90 (2026) 105410

Contents lists available at ScienceDirect

Energy Storage Materials

journal homepage: www.elsevier.com/locate/ensm

Toward room temperature fluoride-ion batteries: quaternary ammonium-bearing fluoride-exchange membrane as a quasi-solid polymer electrolyte

Federico Maria Scesa [a], Maurizio Sansotera [a,b,*], Eugenio Gibertini [a], Sinan Baris Uncu [a], Marco Gregorio [a], Giuseppina Raffaini [a,b], Luca Magagnin [a,b]

[a] Dipartimento di Chimica, Materiali e Ingegneria Chimica, Politecnico di Milano, Via Edoardo Bassini 6, 20131, Milano, Italy
[b] Consorzio Interuniversitario Nazionale per la Scienza e Tecnologia dei Materiali (UdR-PoliMi), via G. Giusti, 9, 50121, Firenze, Italy

ARTICLE INFO

Keywords:
Fluoride-ion batteries
Fluoride-ion exchange membranes
Ionomeric polymers
Quasisolid polymer electrolytes
Molecular dynamics simulations

ABSTRACT

Fluoride-ion batteries (FIBs) are promising alternatives to lithium-based energy storage systems, offering superior electrochemical stability, efficient ion transport, and high elemental abundance. However, the practical application of FIBs is hindered by the lack of efficient solid-state electrolytes with adequate ionic conductivities at room temperature. In this study, we present a novel quasi-solid polymer electrolyte (SPE) in the form of a fluoride-exchange membrane (FEM) based on a perfluorosulfonic amide ionomer with tetraalkylammonium fluoride functional groups. The fluoride-ion conductivity of the polymer electrolyte is enhanced through tailored ionomer swelling using a solvent mixture of 1,3-dioxolane (DOL) and dimethyl sulfoxide (DMSO). Molecular dynamics simulations support the role of DMSO as a polar FEM swelling agent. Electrochemical impedance spectroscopy (EIS) reveals ionic conductivities of up to 1.3×10^{-3} S cm^{-1} at room temperature, with stable cycling performance exceeding 50 cycles in a coin-cell configuration. The electrolyte stability and reversibility are demonstrated by galvanostatic charge-discharge tests using Pb/PbF_2 electrodes, in which reversible fluorination/defluorination at ±0.8 V with a current density of 0.1 C is achieved. These results pave the way for room-temperature applications of FIBs and their future commercialization.

1. Introduction

The global demand for energy storage is increasing, driven by the expanding use of battery-powered devices and the need to transition to sustainable energy. This trend highlights the need for a new generation of electrochemical devices capable of storing more energy while minimizing both economic and social costs. Lithium-based batteries, which dominate the current energy storage market, depend on limited mineral resources, such as lithium itself, cobalt and nickel, which raises environmental and geopolitical concerns [1] In this context, fluoride-ion batteries (FIBs) have emerged as promising alternatives because they combine the distinctive properties of fluoride ions, including their excellent electrochemical stability, efficient transport characteristics, and high abundance, with the high theoretical energy density enabled by fluoride-based conversion chemistry in the electrodes [2] FIBs operate via a rocking-chair mechanism, in which fluoride ions shuttle reversibly between two electrodes with different fluorination and defluorination potentials. However, FIB technology is still at its early stage, and one of the main challenges is the development of electrolytes with a high ionic conductivity at room temperature. In recent years, research has focused mostly on all-solid-state FIBs using ion-conductive ceramic materials based on rare-earth elements, such as barium-doped lanthanum fluoride or barium tin fluoride [3–7] These materials, however, exhibit low ionic conductivities and therefore require high operating temperatures, in addition to having compatibility issues with conversion cathodes due to electrode volumetric expansion during charge-discharge cycles [8–10]

Liquid electrolytes offer high ionic conductivities and superior interfacial contact with electrodes, facilitating the accommodation of expansion and contraction of materials during cycling. However, their practical application is limited by the low solubility of metal fluorides in organic solvents because of the strong ionic nature of fluoride-metal bonds [11] Moreover, in the presence of mildly acidic hydrogen sources, the Lewis basicity of unsolvated fluoride ions (i.e., "naked"

* Corresponding author.
E-mail address: maurizio.sansotera@polimi.it (M. Sansotera).

https://doi.org/10.1016/j.ensm.2026.105410
Received 15 April 2026; Received in revised form 10 July 2026; Accepted 23 July 2026
Available online 24 July 2026
2405-8297/© 2026 The Authors. Published by Elsevier B.V. This is an open access article under the CC BY-NC-ND license (http://creativecommons.org/licenses/by-nc-nd/4.0/).

Table 1
Summary of state-of-the-art electrolytes for FIBs and their key performance metrics: ionic conductivity, working temperature and maximum number of cycles.

Type	Electrolyte	Ionic Conductivity (S cm^{-1})	Temp. (°C)	No. of cycles	Ref.
Solid	$La_{0.9}Ba_{0.1}F_{2.9}$	$2.8 \cdot 10^{-4}$	160	10–22	[4]
Liquid	Sx:CsF:TPhBx	$4.6 \cdot 10^{-4}$ / $1 \cdot 10^{-3}$	25/55	3/10	[10]
Liquid	G4:CsF:TPhBx	n.d.	25	3	[14]
Liquid	Np_2F/BTFE	$2.2 \cdot 10^{-3}$	25	7–10	[15]
Liquid	CsF 37 m in H_2O	> 0.1	25	50	[13]
Liquid/ Gel	PEG:NH_4HF_2	$2.1 \cdot 10^{-3}$	25	1[a]	[16]
Polymer	PVA:Glycerol: Borax	$1.1 \cdot 10^{-3}$	60	60	[17]
Polymer	PEO:MF:TPhBX	$1.1 \cdot 10^{-6}$	25	n.d.[b]	[18]
Polymer	Modified-ionomer in DMSO:DOL 30:70	$1.3 \cdot 10^{-3}$	25	50	*

n.d. not determined.
[a] discharge only.
[b] only ion conductivity.
* this work.

fluorides) promotes the degradation of solvents and fluoride counterions, with the formation of highly corrosive hydrofluoric acid (HF) [12,13] additionally, common battery electrolytes bearing electrophilic groups (e.g., C═O, C≡N and O—C═O) decompose due to side reactions with fluoride ions.

Several strategies have been explored to address these limitations, including the use of aqueous-based electrolytes in solvent-in-salt conditions and boron-based anion acceptors to increase CsF solubility in organic solvents [9–11,13,14] Promisingly, as proposed by Davis et al., several tetraalkylammonium fluorides dissolved in a partially fluorinated ether have been tested in FIBs, showing high ionic conductivities, good chemical and electrochemical stabilities, and reversibility of Cu/CuF_2 fluorination/defluorination [15]

Only a few attempts have been made to use polymer electrolytes in FIBs: [16–18] a liquid electrolyte made of ammonium bifluoride was embedded in a solid polyethylene-glycol matrix, improving the ionic conductivity but without providing reversible cycling; a polyvinyl alcohol-borax-glycerol polymer electrolyte enabled reversible cycling with a sufficient conductivity only above room temperature. State-of-the-art electrolytes for FIBs and their key performance metrics were summarized in Table 1.

Despite these advances, a fundamental gap remains between highly conductive liquid electrolytes, which suffer from chemical instability and salt-solubility constraints, and solid polymer electrolytes, which typically exhibit insufficient fluoride-ion conductivity at room temperature. Quasi-solid polymer electrolytes (QSPEs) can offer a potential intermediate solution by combining the mechanical integrity and safety of solids with the interfacial compliance and enhanced ion mobility of liquids. In this work, a QSPE based on a perfluorosulfonic amide ionomer bearing tetraalkylammonium fluoride was synthesized and used as a fluoride-exchange membrane (FEM) for assembling FIBs operating at room temperature. Perfluorinated ionomers are already employed as cation-exchange membranes in fuel cells, demonstrating performance and stability exceeding 10.000 h [19] By converting these ionomers into anion-exchange membranes through the introduction of hydrogenated spacers bearing ammonium moieties, they can also be used in alkaline electrolyzers [20–22] The stability of the FEM in an FIB mainly depends on its reactivity with fluoride ions, which can be significantly suppressed by properly designing the hydrogenated spacer bearing ammonium groups, thus inhibiting the Hoffmann elimination reaction in particular. For this purpose, *N,N*,2,2-tetramethyl-1,3-propanediamine, characterized by the absence of hydrogen atoms at the β-positions of the ammonium group, was used as an amine for the synthesis of a perfluorosulfonic amide polymer employed as an FEM in FIB assembly. After methylation with methyl tosylate followed by ion exchange with potassium fluoride (KF), tetraalkylammonium fluoride end groups were obtained as the termini of the perfluorosulfonic branches. The synthesis was confirmed by attenuated total reflectance-Fourier transform infrared (ATR-FTIR) analysis and solid-state nuclear magnetic resonance (ssNMR) spectroscopy.

Adequate FEM swelling resulted in maximization of the exploitation of the ionomeric end groups available in the electrolytic membrane; in addition, strong solvation of fluoride ions reduced F^- reactivity, therefore extending the QSPE lifespan. 1,3-Dioxolane (DOL) was used as the main solvent, acting as a coelectrolyte and an FEM swelling agent, because of its polarity, low viscosity, wide stability window, and widespread use in electrochemical applications [23,24] Dimethyl sulfoxide (DMSO) was added at various weight ratios as a highly polar additive [25] Because solvent-induced swelling governs both the nanoscopic organization of the ionomer and the accessibility of fluoride-transport pathways, molecular dynamics (MD) simulations of FEM swelling in the presence of DOL and DMSO were employed to elucidate the relationship between solvent composition, ionomer structure, and ionic transport [26,27]

The ionic conductivity and electrochemical stability window of the swollen FEM were measured via electrochemical impedance spectroscopy (EIS) and linear sweep voltammetry (LSV), respectively. The cyclability was tested at room temperature in a coin-cell setup via galvanostatic charge–discharge with a pseudo-reference Pb/PbF_2 electrode, and the results demonstrated reversible fluorination/defluorination within a voltage window of ±0.8 V vs. PbF_2/Pb at a constant current of 0.1 C (i.e., 22 mA g^{-1}). This assembly, in which a swollen ionomeric polymer electrolyte is used to achieve an adequate ionic conductivity, represents a novel approach in the field of FIBs, opening new perspectives for the development of stable and efficient reversible FIBs operating at room temperature.

By correlating molecular-level structural insights from MD simulations with experimental swelling behavior, ionic conductivity, and electrochemical performance, this work established a structure-mechanism-performance framework for the rational design of a QSPE for room-temperature FIBs.

2. Materials and methods

2.1. Materials

N,N,2,2-Tetramethyl-1,3-propanediamine (Merck, 97%) and Aquivion® DB79-BS (Syensqo, 25% aqueous suspension, equivalent weight (EW) of 790 g/mol) were used as received. CsF (Merck, 99%) and methanol (Merck, 99.8%) were used for the preparation of a reference electrolyte. Dimethyl sulfoxide (DMSO) (Merck, 99.9%, anhydrous), 1,3-dioxolane (DOL) (Merck, 99.8%, anhydrous) and bis(2,2,2-trifluoroethyl) ether (BTFE) (Merck, 98%) were opened and stored under an inert atmosphere. 2-Propanol (Merck, 99.5%), N,N-dimethylacetamide (Merck, for synthesis), anhydrous acetonitrile (Merck, 99.8%), methyl tosylate (Merck, 97%), and KF (Merck, >99%) were used. PbF_2 (Merck, >99%), Super P® (Thermo Fisher, >99%), lead acetate (Thermo Fisher, 98%), Galden® HT perfluoropolyether (Solvay Specialty Polymers) and Hyflon AD60® (Solvay Specialty Polymers) were used for electrode preparation. Coin cells were assembled in an Ar-filled glovebox with O_2 and H_2O contents of <0.5 ppm. To determine the ionic exchange capacity, pentafluorobenzyl bromide (Merck, for synthesis), chlorobenzene (Merck, 99.5%) and acetone (Carlo Erba, RE, Puro) were used as received.

2.2. Methods

2.2.1. Quasi-solid polymer electrolyte synthesis

A quasi-solid polymer electrolyte (QSPE) was synthesized by adapting the procedures from Bonizzoni et al. and Stilli et al. [20,21] The typical preparation of a polymer electrolyte consisted of mixing a perfluorosulfonic acid resin in the form of an aqueous or hydroalcoholic dispersion with 2-propanol, *N,N*-dimethylacetamide and 3 equivalents of *N,N*,2,2-tetramethyl-1,3-propanediamine (henceforth referred to as diamine) to obtain a stable dispersion with 12% wt. of the polymer (Step 1). The dispersion was poured into a glass Petri dish to obtain a 50–80 μm thick membrane; then, the membrane was dried under nitrogen flow at 50 °C for 6 h and sintered at 250 °C for 1 h at a heating rate of 180 °C/h to form a sulfonamide bond (Step 2).

For the alkylation step, the sintered membrane was peeled from the Petri dish and soaked in anhydrous acetonitrile in a polytetrafluoroethylene (PTFE)-lined stainless-steel autoclave under inert conditions; then, a large excess (≈10 equivalents) of methyl tosylate was added to obtain the ammonium salt (Step 3). The autoclave was heated at 60 °C for 20 h. After the reaction was completed, the membrane was washed with acetonitrile and water. Thereafter, the tosylate counterion was exchanged with the fluoride ion by immersing the membrane for 24 h in a 1 M KF aqueous solution (Step 4). The fluoridated membrane was washed with deionized water and then dried under vacuum for 6 h at 50 °C; prior to storing membranes were washed three times with anhydrous solvent under inert conditions; then, it was stored in the liquid co-electrolyte and conditioned for at least 24 h before being utilized for cell assembly. The fluoride-exchange membrane (FEM) was characterized after each synthetic step by Fourier transform infrared (FTIR) analysis in attenuated total reflectance (ATR) mode and [13] C-^{1}H cross polarization/magic angle spinning nuclear magnetic resonance (CP/MAS NMR) spectroscopy. The characterization results are discussed in Section 3.

2.2.2. Reference electrodes

Lead nanoparticles were obtained by thermal decomposition of lead acetate in an alumina crucible at 550 °C for 20 min under Ar flow and were stored under Ar [12]

Lead fluoride was preliminarily milled for 3 h at 250 rpm to reduce and homogenize the particle size using a TOB–ZQM Series high-speed planetary ball mill. The crystalline phase of the ball-milled powder was verified by XRD (Philips PW 1830 diffractometer equipped with a Bragg Brentano goniometer and Cu-Kα_1 radiation), confirming the orthorhombic α-PbF_2 polymorph (Figure S1 in the Supporting Information). Then, PbF_2 was mixed with Super P® as a conductive additive, Hyflon AD60® as a perfluorinated polymeric binder, lead powder and a perfluorinated solvent (Galden® HT perfluoropolyether) at proportions of 45% Pb, 40% PbF_2, 10% Super P® and 5% Hyflon AD60®. The mixture was mechanically milled at 200 rpm for 30 min, and the obtained ink was coated on a graphite sheet with a 100 μm wet thickness. The electrode sheets were dried for 12 h at room temperature and 4 h at 50 °C under vacuum. The electrode was subsequently cut and stored under an inert atmosphere.

2.3. Characterization techniques

2.3.1. Chemical-physical characterization

Solid-state [13] C-^{1}H CP/MAS NMR was used to confirm FEM functionalization with the diamine: 20k scans were acquired by a Brucker Advance II 500 MHz spectrometer with a relaxation time (D1) of 2.5 ms and a contact time (P1) of 1 s. The sample was cut into small pieces, placed in a 4 mm zirconia rotor with a KelF cap, and spun at 10 kHz.

FTIR spectra were acquired in ATR mode with a Nicolet iS10 equipped with an ATR Smart iTR module and a zinc selenide crystal in the 4000–400 cm^{-1} range with 64 scans at a 4 cm^{-1} spectral resolution. All the samples were dried under vacuum at 60 °C for 12 h before analysis.

The ion exchange capacity (IEC) was determined by gas chromatography-mass spectrometry (GC–MS), adapting a method from Kage and coworkers [28] Their approach was based on the derivatization of inorganic halide ions into detectable volatile organic derivatives through nucleophilic substitution, allowing their separation by gas chromatography and subsequent quantification by mass spectrometry. In the present work, this method was adapted for IEC evaluation in a solid electrolyte. Therefore, the membrane was converted to its chloride form after quaternarization of the amine groups (step 3 of the membrane synthesis), instead of its fluoride form. In fact, the use of fluoride ions could lead to an IEC underestimation due to F^- strong interaction with quaternary ammonium groups, which may hinder complete ion exchange and quantitative derivatization. For IEC determination, the fluoridation step (step 4 of the membrane synthesis) was replaced by a chloride exchange, whereby the tosylate counterions were exchanged with the chloride ions by immersing the membrane for 24 h in a 1 M NaCl aqueous solution. Then, it was washed with deionized water and dried it under vacuum for 6 h at 50 °C. Chloride ions were subsequently exchanged with nitrate ions and at this stage the released Cl^- were quantified in the aqueous phase using pentafluorobenzyl bromide as a derivatizing agent and chlorobenzene as an internal standard. Typically, a small amount of dried membrane (15–25 mg) was immersed in 0.5 ml of 0.2 M KNO_3 solution. After 24 h, 0.1 ml of solution and 0.2 ml of 0.2 M phosphate buffer (pH 6.8) were added to a 3 ml glass vial. Then, 0.5 ml of a 300 mM solution of pentafluorobenzyl bromide in acetone was added, and the closed vial was heated at 80 °C for 1 h. After 1 h, the sample was cooled at room temperature, and 1 ml of a 0.2 mM solution of chlorobenzene in *n*-hexane was added and stirred for 1 min. After phase separation, 1 μl of organic phase was injected into the GC–MS instrument, an Agilent GC 6850 equipped with an HP-5MS column and coupled with an Agilent MSD 5975C detector operating in single-ion monitoring mode (Table S1) calibrated on fragments with *m/z*equal to 216 for perfluorobenzyl chloride and 112 for chlorobenzene as an internal standard.

The reference solutions containing chloride were prepared at concentrations ranging from 10 to 200 ppm. The calibration curve was constructed by plotting the concentrations of the reference solutions in ppm against the peak-area ratio of the molecular peak of the chloride derivative at *m/z*216 to the base peak of chlorobenzene at *m/z*112 (Fig. S2). The equation of the calibration curve was $y = 106.41 \times 46.596$ ($r = 0.996$), which was used to quantify the amount of chloride ions exchanged by the membranes. The final IEC value was calculated as follows:

$$IEC = \frac{n\ of\ chloride\ ions\ exchanged\ (meq)}{dry\ membrane\ mass\ (g)}$$

The equivalent weight (EW) of the FEM can be calculated directly from the IEC value according to:

$$EW = \frac{1}{IEC} \cdot 1000$$

2.3.2. Electrochemical characterization

All the electrochemical tests were performed on AISI 316 stainless steel CR2025 coin cells assembled in an Ar-filled glovebox. The ionic conductivity was determined by performing electrochemical impedance spectroscopy (EIS) on ionomeric membranes placed between two stainless steel blocking electrodes in a custom-made Swagelok-type cell (Fig S3) [29] The FEMs were conditioned for at least 12 h in the swelling mixture. The impedance spectra were recorded with a Biologic VSP300 at frequencies between 5 MHz and 0.100 Hz, with a 5 mV perturbation. The bulk resistances were calculated from experimental data fitted with the ZFit tool in Biologic EC-Lab Software using a Debye circuit as an equivalent circuit model (inset in Figure), which was composed of a

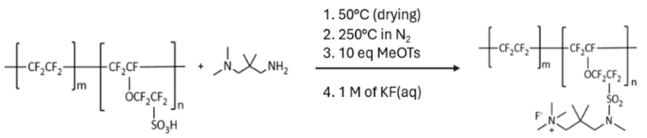


Fig. 1. Reaction scheme for FEM synthesis.

constant-phase element that models the dielectric capacitance in parallel with a resistor that models the ionic resistance of the membrane in series with another constant phase element that represents the double-layer capacitance.

Galvanostatic cycling was performed using a Neware battery cycler and Neware BTS software. The coin cells were assembled in a symmetric configuration with two Pb/PbF_2 electrodes separated by the QSPE. Graphite sheets were used as current collectors to avoid contact between the FEM and the stainless-steel coin cell, thereby minimizing possible corrosion and parasitic reactions induced by fluoride ions, and reducing undesired contributions to the electrochemical response Fig. 1.

Before the cells were sealed, 15 μl of a swelling agent was added to ensure that both the membrane and the electrodes remained completely wet. The cells were allowed to rest for 24 h after assembly, after which the cycling steps consisted of galvanostatic charging followed by galvanostatic discharging with a potential limit of ± 0.8 V. For consistency, the data discussed were obtained using membranes and electrodes prepared from the same batch. Benchmark cells were built using a reference electrolyte made with CsF 10 m in methanol and two Cellgard 2325 polypropylene membranes as separators Fig. 2.

2.4. Molecular mechanics (MM) and molecular dynamics (MD) simulations

This theoretical study at the atomistic level was based on molecular mechanics (MM) and molecular dynamics (MD) simulations performed to describe the influence of different solvent mixtures on the conformational properties of a single ionomer chain and the bulk properties of 30 ionomer chains in a simulated box and in the presence of pure DOL or pure DMSO. All simulations were performed using the Materials Studio 7.0 and Discovery Studio 2020 packages (version 7.0, BIOVIA, Accelrys Inc., San Diego, CA, USA) and the CVFF force field [30,31]

The conformational properties of the ionomer chains with m/n equal to 3.5 and 6 side chains were studied by considering a single chain with or without DOL and DMSO solvent molecules at different ratios, as reported in Figure S4. Specifically, a single ionomer chain was studied without a solvent (Figure S4b), with 8 DOL molecules (Figure S4c), with 21 DOL and 2 DMSO molecules (Figure S4d), with 22 DOL and 9 DMSO molecules (Figure S4e), and with 41 DMSO molecules (Figure S4f). Similar to previous theoretical studies, [26,27] the simulation protocol consisted of three steps: i) energy minimization in vacuo of the initial geometries of the isolated ionomer chain or ionomer chain in the presence of solvent molecules with initial random arrangements in a simulation box; ii) NVT (constant number of particles, volume, and temperature) MD runs at T = 300 K lasting 10 ns until an equilibrium state was achieved, with analysis of the 1000 conformations of the

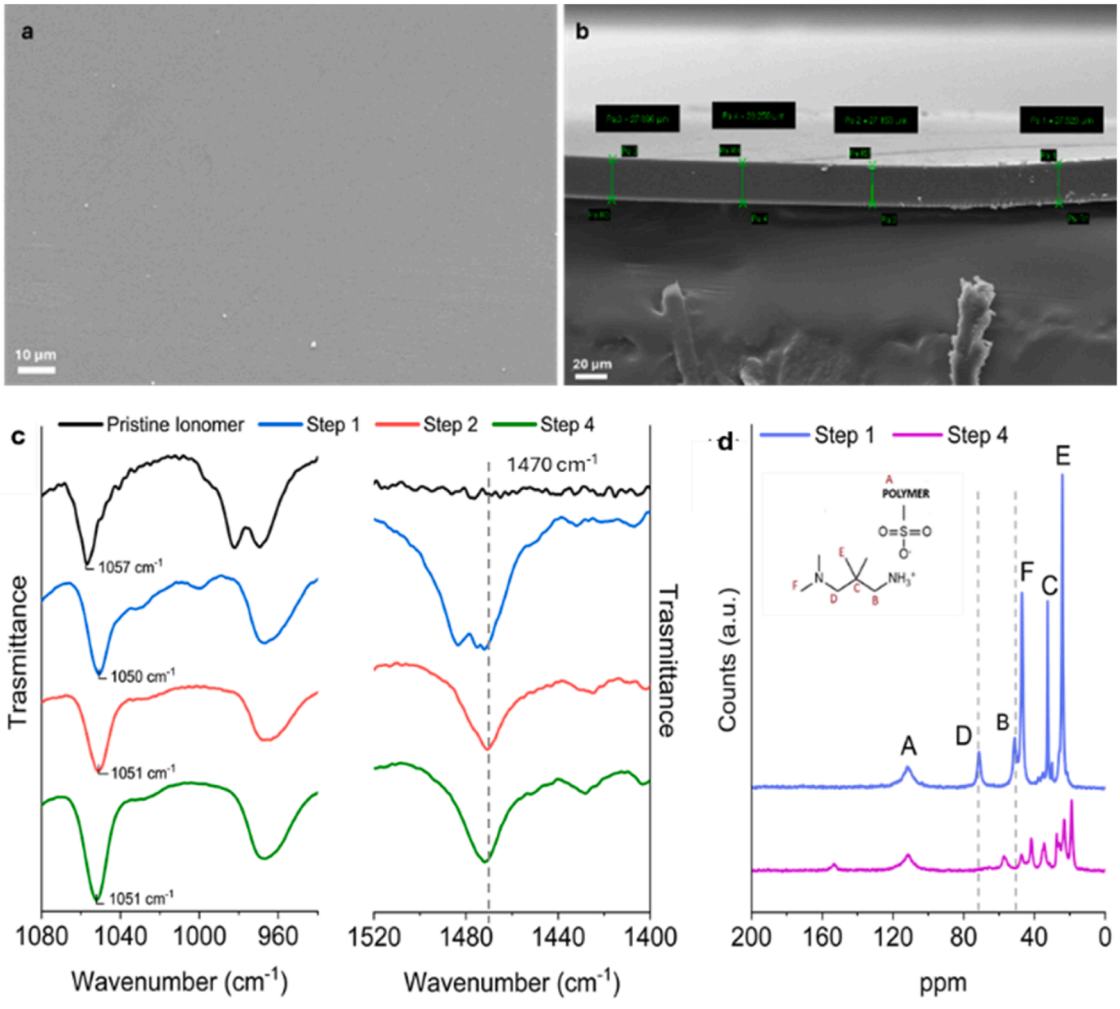


Fig. 2. SEM images of casted FEM, detail of surface (a) and cross-section profile (b), ATR-FTIR spectra (c) and.^{13}C-^{1}H CP-MAS spectra (d).

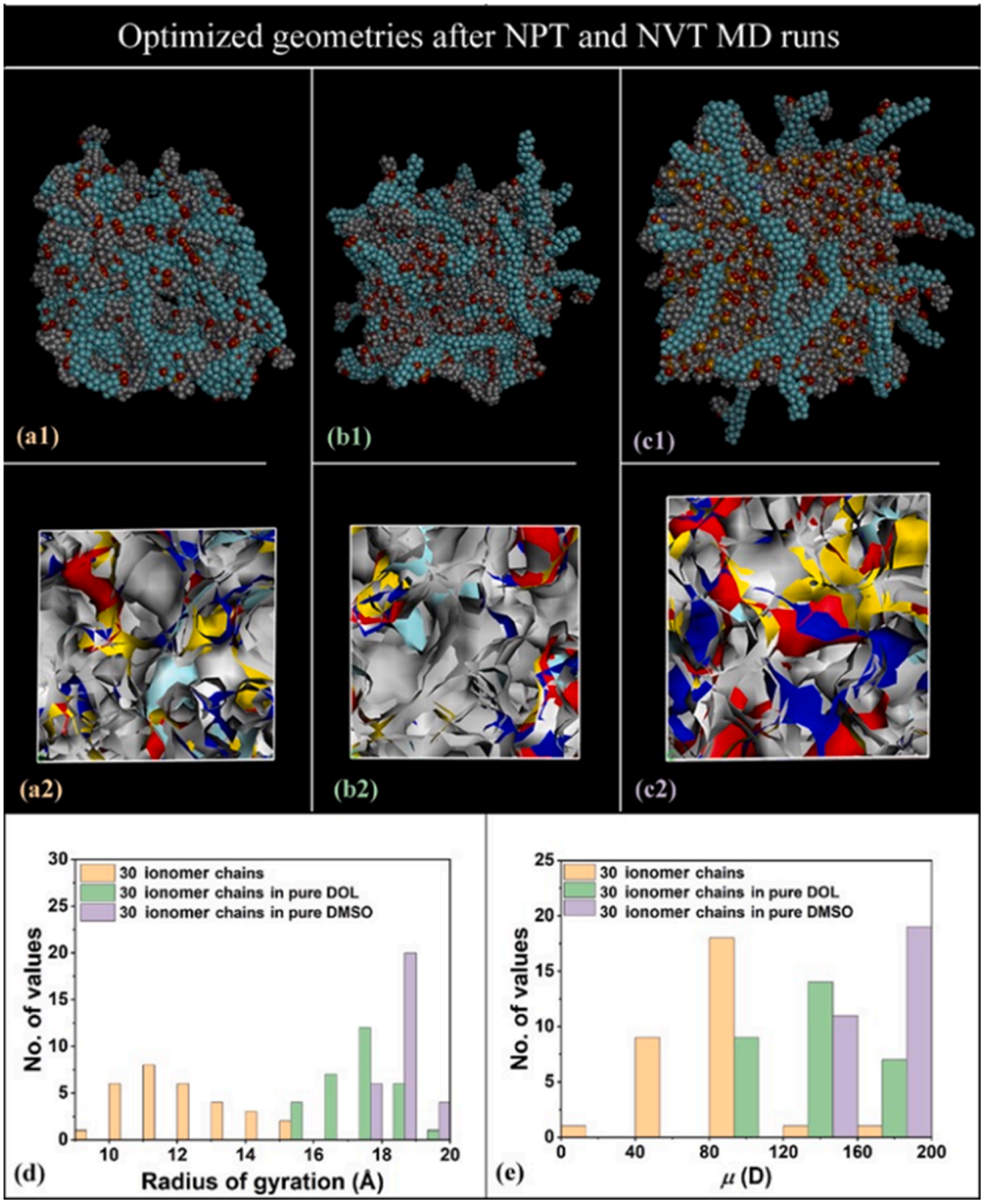


Fig. 3. Optimized geometries of 30 ionomer chains after NVT and NPT MD runs (a1). Final optimized geometries of 30 chains in pure DOL (b1) and pure DMSO (c1), respectively. The edges of the cell are omitted for clarity. The carbon atoms are gray, the nitrogen atoms are blue, the fluorine atoms are light blue, the oxygens are red, and the sulfur atoms are yellow. Density fields (a2), (b2), and (c2) calculated for the atoms of the ionomer chains only for the three different optimized geometries reported in panels (a1), (b1), and (c1), respectively. Distributions of the radius of gyration, R_g, of the ionomer chains (d) and their dipole moments (μ) (e) calculated for the optimized geometries reported in panels (a1), (b1), and (c1). All data shown in this figure were obtained from the first MD simulation run.

systems saved every 10 ps; and, finally, iii) geometry optimization of the system at the end of the MD runs and for selected instantaneous frames saved during MD runs. All energy minimizations were performed using the conjugate gradient algorithm until the energy gradient was reduced to below $4{\cdot}10^{-3}$ kJ mol^{-1} Å^{-1}. All NVT MD simulations were performed at a constant temperature, T = 300 K, controlled through a Berendsen thermostat. The dynamic equations were integrated using the Verlet algorithm with a time step of 1 fs. The equilibration state was monitored by following the evolution of the potential energy and its components from an energetic point of view and the evolution of selected geometrical parameters over time, specifically, the radius of gyration (R_g) and the dipole moment. The radius of gyration, R_g, of the ionomer chain isolated or solvated in different DOL and DMSO solvent mixtures was calculated during the five different MD runs for 10 ns, as reported in Figure S4a. For a statistical analysis related to the conformational study of the ionomer chain as is or in the presence of DOL or DMSO molecules or their mixtures, two further MD runs were carried out for each case studied following the simulation protocol reported above. The probability densities related to the radius of gyration, R_g, of the ionomer chain isolated or solvated in different DOL and DMSO solvent mixtures,

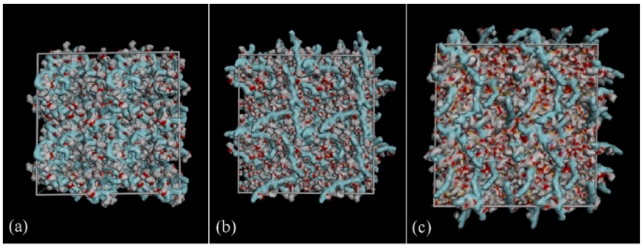


Fig. 4. FASAs calculated for the optimized geometries of 30 ionomer chains in the FEM bulk without solvents (a), in pure DOL (b) and pure DMSO (c), respectively, by multiplying axes a, b, and c by 2. The probe has the same diameter as the fluoride ion. The color code is the same as that in Fig. 3. All data shown in this figure were obtained from the first MD simulation run.

calculated during the three MD runs lasting for 10 ns performed for each system studied, are reported in Figure S5.

The conformational properties of 30 ionomer chains in the FEM bulk without a solvent and their behavior in pure DOL and pure DMSO were evaluated by a specific two-step simulation protocol. The first step of this procedure involved the following steps: I) energy minimization of the system within a cubic simulation box with a side length of 250.0 Å considering periodic boundary conditions, followed by NVT MD runs of 10 ns, with geometry optimization of the system performed at the end of every MD run; II) NPT (constant number of particles, pressure equal to 0.1 GPa, and temperature equal to 300 K) MD runs of 1 ns and energy minimization of the system at the end of every MD run, with optimization of the cell parameters; and III) NPT (constant number of particles, pressure equal to 1 GPa, and temperature equal to 300 K) 1 ns MD runs and energy minimization of the system at the end of every MD run, with optimization of the cell parameters. The second step of this procedure started from the optimized geometries obtained at the end of the first step. This step was aimed at further investigating the conformational properties of 30 ionomer chains in the FEM bulk, both in the presence and absence of pure DOL or DMSO molecules. This step involved the following steps: NVT (constant number of particles, volume, and temperature) MD runs at T = 500 K for 500 ps; NVT MD runs at T = 400 K for 500 ps; NVT MD runs at T = 300 K for 1 ns; and NVT MD runs at T = 300 K for 2 ns. Here, geometry optimization of the system was performed at the end of every MD run under all conditions. All NPT MD simulations were performed at a constant temperature, which was controlled using a Berendsen thermostat and barostat. The evolution of the potential energy and its components were calculated during MD runs from 1000 frames periodically saved. The final optimized geometry containing 30 ionomer chains in a simulation cell with edges measuring 64.5 Å × 62.7 Å × 63.5 Å (omitted for clarity) is reported in Fig. 3 a1. The final optimized geometry related to 30 ionomer chains in pure DOL (240 DOL molecules) in a simulation cell with edges equal to 63.1 Å × 64.1 Å × 64.6 Å (omitted for clarity) is reported in Fig. 3 b1. The final optimized geometry related to 30 ionomer chains in pure DMSO (1230 DMSO molecules) in a simulation cell with edges equal to 69.7 Å × 69.6 Å × 69.4 Å (omitted for clarity) is reported in Fig. 3 c1.

The concentration profile was calculated for 3D periodic structures by analyzing the atom density distribution within evenly spaced slices parallel to the bc, ca, and ab planes for the structures reported in panels (a), (b), and (c) in Figure S6.

After the axes a, b, and c of the structures obtained at the end of the procedure reported in Fig. 3 were doubled and the energy of the resulting system was minimized, the FASA (i.e., fluoride accessible surface area) was determined, as shown in Fig. 4, using a probe with a radius equal to half that of the fluoride ion (0.7 Å). The color code corresponds to the atomic colors depicted in Fig. 3. For the statistical analysis of the FASA of 30 ionomer chains in the FEM bulk in absence of solvent, in pure DOL and pure DMSO, two further MD runs lasting for 2 ns were performed for each case studied starting from the optimized geometries obtained as described above, and the FASA were calculated for each of the independent MD runs.

3. Results and discussion

3.1. FEM preparation and characterization

Ionomers are a class of copolymers in which one monomer contains an ionic group, and their functionality is due to acid groups that allow exchange of H^+ ions or metal cations [32] They are widely used as ion-exchange resins, catalysts, and membranes and play crucial roles in energy storage and production applications, such as in electrolyzers, fuel cells, and redox flow batteries. The polymer backbone, which provides structural and mechanical stability, can be either hydrogenated (e.g., sulfonated polyetheretherketone, sPEEK) or fluorinated (e.g., perfluorosulfonic acid resins, PFSAs) [33,34] PFSA-based ionomers are the most widely used materials in electrochemical applications because of their excellent chemical, electrochemical, and thermal resistance.

PFSA ionomers are classified according to the structure of their side chains, which carry ionic groups. The first PFSA ionomers were introduced by DuPont under the trade name Nafion® and featured long-side-chain (LSC) structures [35] Later, short-side-chain (SSC) ionomers were developed, which exhibited higher crystallinity at the same equivalent weight (EW), allowing a decrease in the EW with improved mechanical properties [36]

In this work, an SSC ionomer was chosen as the starting material because of its higher crystallinity and lower equivalent molecular weight than those of other PFSA membranes. Initially, the SSC ionomer contained -SO_3H groups and was characterized by a cation-exchange property. The -SO_3H groups were successfully amidated using *N,N*,2,2-tetramethyl-1,3-propanediamine, and the free amine group remaining after sulfonamide formation was subsequently methylated with methyl tosylate, forming ammonium end groups that behaved as anion carriers. Fig. 1 shows the reaction scheme, the detailed preparation method is outlined in the previous section. This process effectively converts the ionomer from a cation-exchange material to an anion-exchange material, making it suitable for providing fluoride-ion conductivity while preserving its structural integrity. The choice of the diamine was crucial because of the absence of hydrogen atoms at the β-position of the ammonium group. This characteristic is particularly important in FIB electrolytes that contain highly nucleophilic unsolvated nucleophilic F^- ions. Under these conditions, β-hydrogens in the diamine structure can easily lead to Hoffmann elimination, quickly degrading the ion-carrier moieties and compromising the FEM lifespan and overall FIB performance.

FEM membrane was observed through SEM and this analysis showed a flat and homogeneous surface morphology, with small defects due to dust or entrapped air bubbles (Fig. 2a). A homogeneous membrane thickness of approximately 28 μm was measured observing the cross-sectional images obtained by brittle fracture of the sample after liquid nitrogen freezing (Fig. 2b). Pictures of the membrane before and after swelling with 30% DMSO DOL solution were also added in the Supporting Information (Fig. S7).

FTIR spectra in ATR mode (Fig. 2c) were acquired after each step of the FEM preparation (full ATR-FTIR spectra and magnifications of the 4000–2500 cm^{-1} region were reported in Figure S8): ionomer and diamine mixing, with ammonium sulfate formation (Step 1); sulfonamide synthesis (Step 2); ammonium formation via methylation (Step 3); and counterion exchange, i.e., fluoridation (Step 4). A redshift from 1057 cm^{-1} to 1050 cm^{-2} was clearly visible in the fingerprint region for the -S–O stretching of the -SO_3X group after Step 1 (formation of an ammonium salt between -SO_3H groups and the diamine). A slight blueshift from 1050 to 1051 cm^{-2} was observed after sulfonamide bond formation in Step 2, whereas no spectral changes were detected after methylation and counterion exchange (Step 4). The peak at around 970 cm^{-1} can be attributed to the bending of the C–O–C bond in the side

chains of the perfluorinated ionomer, which remained unaffected by functionalization. These results were consistent with data previously reported in the literature for similar systems [21,22] Additionally, the C—H bending region was featureless in the pristine ionomer, whereas after diamine treatment, a peak emerged at approximately 1460–1470 cm^{-2}, corresponding to the bending vibrations of the -CH_3 and -CH_2- groups in the diamine. In Figure S8, aliphatic C–H stretching bands were clearly visible in the 2960–2760 cm^{-1} region, confirming the incorporation of the diamine-derived spacer into the membrane; in contrast, the characteristic NH_2 stretching doublet of the free diamine was not observed [37] In addition, the broad band at 3000–3500 cm^{-1} evolved significantly during the membrane functionalization process. These observations were consistent with changes in the local chemical environment due to ammonium formation, sulfonamide synthesis, and quaternarization, rather than to the presence of free diamine. It is worth noting that the membranes were dried before the ATR-FTIR analysis (see Section 2.3.1 for details); however, small amounts of strongly retained moisture could remain adsorbed within the membrane due to the highly hygroscopic nature of ionomeric materials.

The ssNMR data confirm the formation of -S-N- bonds, in accordance with assignments previously reported in the literature (Fig. 2d) [20] Specifically, the disappearance of the singlet at 71 ppm (peak D), which corresponds to the carbon atom at the α-position relative to the tertiary amine group, indicates the formation of a sulfonamide bond and quaternarization of the adjacent nitrogen atom. Moreover, the apparent upfield shift of all the peaks in the diamine region (25–50 ppm) further supports the formation of a sulfonamide bond. Additionally, the small peak at approximately 155 ppm after Step 4 is attributed to carbonyl groups originating from reactions with trace CO_2 during the thermal treatment of the membrane. The reaction yield, evaluated by ion exchange capacity (IEC) measurements, was approximately 91.5%, as reported in the Supporting Information.

3.2. MM and MD simulations

Ionomers are widely used in aqueous systems because of their excellent swelling properties; in fact, the distinctive ion transport behavior of PFSA ionomers arises from their phase-separated nanostructure. These polymers consist of a hydrophobic fluorocarbon backbone and hydrophilic domains formed by ionic side chains with hydrated endgroups. According to the model originally introduced by Gierke and Hsu [32,34] the hydrophilic regions aggregate into ionic clusters dispersed within the continuous fluorocarbon matrix. Ion conduction takes place through a network of narrow channels interconnecting these clusters, with both the development and connectivity of this pathway being strongly governed by the membrane's degree of solvatation.

However, the narrow electrochemical stability window of water limits their use in energy storage systems [11,14,15] As a result, polar aprotic solvents have been explored as alternative swelling agents for FIBs. Effective membrane swelling of an FEM promotes solvation of ionomer side chains and connectivity among ionic clusters, maximizing charge carrier utilization and the ionic conductivity.

Davis et al. reported a high-performance liquid electrolyte based on bis(2,2,2-trifluoroethyl) ether (BTFE) and neopentyl ammonium fluoride. However, the low dielectric constant ($\varepsilon \approx 4.4$) of pure BTFE makes it unsuitable for membrane swelling. The salt dissolving properties in solvents for FEMs are secondary to a high dielectric constant to achieve membrane swelling, which facilitates ionic cluster separation and connectivity [38] DMSO was therefore considered because of its high dielectric constant ($\varepsilon = 47$) and pkA (35), which ensures stability under fluorination conditions because it exceeds the fluoride stability threshold (~33) [12] Despite these advantages, the high viscosity and high melting point (19 °C) of DMSO limit its standalone use in electrolyte formulations. Thus, it was blended with DOL, a solvent with a low viscosity, a low melting point and moderate polarity ($\varepsilon = 16$) widely used in Li-ion batteries and supercapacitors [23–25] Accordingly, three representative solvent compositions were selected for the experimental investigation. Pure DOL was used as the reference system, whereas a DMSO:DOL mixture containing 30 wt.% DMSO represented the highest DMSO content that maintained the solvent mixture in the liquid state down to −20 °C while providing sufficient polarity for complete membrane swelling, thereby ensuring adequate ionic conductivity also at low temperatures. A 10 wt.% DMSO composition was also selected as intermediate DOL-rich formulation to evaluate whether a limited addition of DMSO could already provide a significant enhancement in membrane swelling and fluoride-ion conductivity while preserving the favorable physical properties of DOL-rich mixtures.

Electrolyte design is critical in FIB development, and both density functional theory (DFT) and MD simulations are widely used to investigate intermolecular interactions and solvent-ion compatibility. Alshangiti et al. applied MD methods to evaluate solvation in a water-in-salt liquid electrolyte [13] whereas more recently, others used it to study fluoride reactivity in an imidazolinium-based ionic liquid proposed as a solvent for tetramethylammonium fluoride (TMAF) [39] Davis et al. applied MD simulations to compute the solvation free energies of fluoride ions and their counterions in various organic aprotic polar solvents. To identify the most suitable solvent, simulations were performed to obtain computationally generated solvent dipole moments and partial charge distributions, which provided insight into solvation mechanisms in both hydrogenated and partially fluorinated solvents, thus contributing to FIB development [15,40]

In this study, atomistic-level MD simulations were used to examine the effects of DOL, DMSO and their mixtures on the conformations of ionomer chains in the membrane, highlighting how swelling modifies FEM features to realize ionic conductivity. The simulations first focused on a single chain, and conformational changes were assessed by calculating its radius of gyration, R_g (Figure S4a). In particular, the probability density of the R_g related to the single ionomer chain calculated for three different MD runs is centered at 11.54 (± 0.46) Å (Figure S5a). Then, considering the solvated ionomer chain initially randomly arranged in the simulation cell, during the MD runs the solvent molecules migrated short distances toward the ionomer side chains because of favorable intermolecular interactions. In pure DMSO and pure DOL the R_g probability density distributions resulting from the three MD runs were centered at 12.24 (± 0.23) Å and 11.42 (± 0.24) Å, respectively (Figure S5b and S5e). Considering solvent mixtures with 21 DOL and 2 DMSO molecules and with 22 DOL and 9 DMSO molecules, the R_g probability density distributions shifted to 12.70 (± 0.47) Å and 11.79 (± 0.31) Å, respectively (Figure S5c and S5d). Therefore, in DOL:DMSO mixtures, the average R_g increased with increasing DMSO content. These results indicated that pure DOL promoted a more compact conformation, whereas the addition of a small amount of DMSO enhanced chain extension, suggesting a synergistic swelling effect.

The theoretical investigation was extended to 30 ionomer chains, simulating the bulk FEM properties with and without solvents (Fig. 3 a1-c1). The optimized structures showed that DOL promoted fewer cavities in the bulk, whereas DMSO swelled the membrane, resulting in larger cavities and the exposure of ammonium groups. The structural arrangement of the ionomer chains in the FEM also differed by solvent: in DOL, fluorinated chains aligned along one axis and perpendicular to another (Fig. 3 b1), whereas in DMSO, the alignment occurred along a single direction, with the formation of multiple interconnected nanocavities serving as pathways for fluoride ion transport (Fig. 3 c1).

With respect to R_g in bulk conditions, the ionomer chains without solvent appeared randomly arranged with limited cavities, and R_g was nearly 11 Å (Fig. 3d). A statistical analysis on three independent MD runs showed that the R_g in the bulk system was equal to 12.30 (± 1.50) Å. In contrast, pure DOL and DMSO increased the R_g to 17.31 (± 1.02) Å and 18.41 (± 0.53) Å, respectively, confirming that both solvents promote the ionomer chain extension, with DMSO producing the largest effect. In addition, the dipole moments of the ionomer chains in the FEM

Table 2
Ionic conductivity at room temperature and Arrhenius parameters in different DMSO/DOL mixtures from EIS measurements.

DOL:DMSO mixture	σ_{298K} (S cm^{-1})	σ_0 (S cm^{-1})	E_a (eV)	$\Delta m_{\%}$ (%)
0% DMSO	4.5 (± 0.8) · 10^{-6}	22 ± 2	0.39 ± 0.02	15
10% DMSO	2.6 (± 0.2) · 10^{-4}	298 ± 3	0.36 ± 0.03	69
30% DMSO	1.3 (± 0.9) · 10^{-3}	2.4 ± 1.7	0.20 ± 0.01	119

bulk increased from 80 Debye with DOL to 200 Debye with DMSO (Fig. 3e), reflecting greater chain extension and increased nitrogen exposure, which are consistent with the observed ionic conductivity improvements.

The fluoride accessible surface areas (FASAs) were calculated for the ionomer chains in the simulated FEM (Fig. 4). The calculated FASA values for the 30 ionomer chains in the absence of solvent, in pure DOL, and in pure DMSO were 529,541 (± 1001) Å^2, 541,750 (± 678) Å^2, and 560,609 (± 1787) Å^2, respectively. These values were obtained from three independent MD runs and indicated that the FASA increased by approximately 3% in pure DOL, whereas by approximately 6% in pure DMSO compared with the unsolvated system. Therefore, DMSO swelling promoted fluoride ion transport among more extended fluorinated chains and swollen side chains, with positively charged nitrogen atoms exposed to the solvent, reflecting experimental observations of membrane swelling. Considering the small size of the fluoride ion, the higher degree of swelling may provide more accessible transport pathways around the ionomer chains. The larger FASA obtained in DMSO resulted consistent with the greater chain extension observed from the R_g analysis.

Notably, the different polarities of DOL and DMSO resulted in different arrangements of solvated ionomer chains. The density fields for the solvent atoms revealed that the oxygen atoms of the less polar DOL molecules were exposed and that the nonpolar groups were more extended toward the ionomer chains (Figure S9a). In contrast, the oxygen and sulfur atoms of the more polar DMSO molecules were exposed to the ionomer chains, enhancing solvation of the polar nitrogen atoms in the ammonium groups (Figure S9b), which resulted in greater accessibility to the solvent, thereby increasing the fluoride-ion conductivity. The concentration profiles of the ionomer chains with solvent molecules confirmed the formation of connected cavities, particularly with DMSO.

Overall, membrane swelling with DMSO promoted ionomer chain extension, ammonium group exposure, directional alignment and cavity formation, which are critical features for fluoride ion conduction. These MD results support the role of DMSO as an effective polar swelling agent for FEMs, in agreement with experimental findings. However, pure DMSO alone would be insufficient to achieve good performance due to its relatively high melting point (19 °C); therefore, DOL was added to the solvent mixture to extend its liquid range to lower temperatures and to enhance the overall transport properties owing to its lower viscosity.

3.3. Ionic conductivity measurements and electrochemical testing

The ionic conductivity at room temperature (σ_{298K}) and Arrhenius parameters (i.e., preexponential factor, σ_0, and activation energy, E_a) were determined for FEMs swollen with several DMSO:DOL mixtures using EIS measurements to assess their temperature-dependent ion transport properties (Table 2). Data were collected in a temperature range between −20 °C and 70 °C (Fig. S10), and the Nyquist plot was fitted with a modified Debye circuit (Fig. 5a). The same temperature range and fitting protocol were consistently applied to all compositions, ensuring that the extracted Arrhenius parameters are directly comparable across different DMSO:DOL ratios.

The σ_{298K} values obtained by EIS measurements confirmed the role of DMSO as a polar additive that increased the ionic conductivity across the membrane. As expected, an increase in the DMSO concentration in the coelectrolyte mixture directly improved the ionic conductivity. Specifically, increasing the DMSO concentration from 10% to 30% increased σ_{298K} approximately by an order of magnitude, from 2.6 10^{-4} to 1.3 10^{-3} S cm^{-1}. This result can be rationalized by considering the Arrhenius parameters: although the membrane swollen with 30% DMSO exhibited a lower pre-exponential factor, σ_0, indicative of a reduced effective concentration of mobile charge carriers on a logarithmic scale, this effect was more than compensated by a substantial decrease in the activation energy, which was nearly halved compared to the 10% DMSO sample (0.20 vs 0.36 eV). Nevertheless, both the 10% and 30% DMSO solutions notably displayed ionic conductivities in the range 10^{-3}–10^{-4} S cm^{-1}, comparable to the values reported for in the literature the best performing alkylammonium fluoride-based liquid electrolytes [15] These values were also two to three orders of magnitude higher than those observed for the membrane swollen in pure DOL, highlighting the crucial role of DMSO in promoting fluoride ion transport.

In Table 2, the solvent uptake ($\Delta m_{\%}$) was also reported: it was defined as the relative mass increase of the membrane after 24 h of equilibration in the corresponding solvent mixture. Higher $\Delta m_{\%}$ values

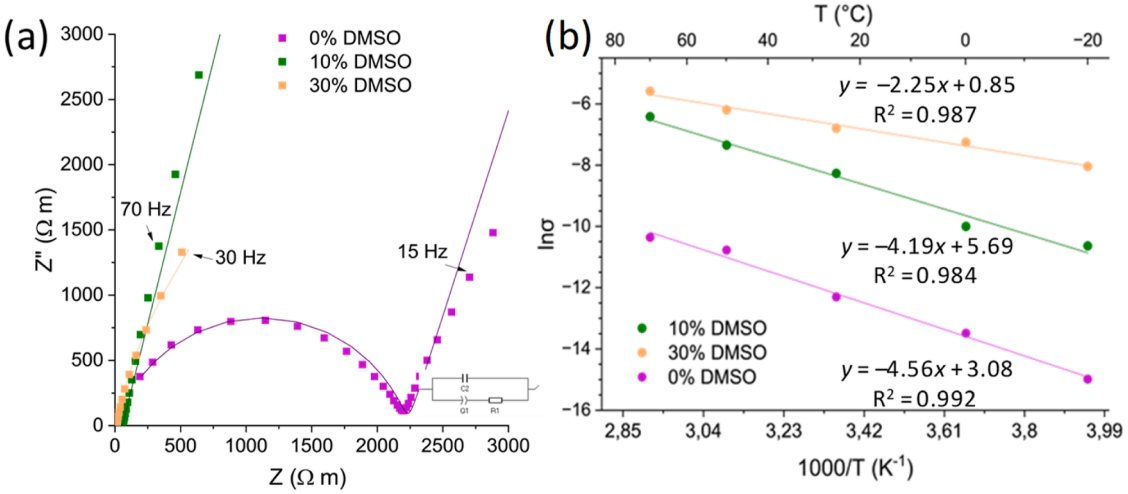


Fig. 5. Nyquist plot for the QSPEs at room temperature (298 K) (a), and Arrhenius plot of the QSPEs (b) swollen with different DOL/DMSO mixtures (linear regression equations and R^2 values were reported in the Figure, and p-values were on the order of 10^{-4} for all the fits).

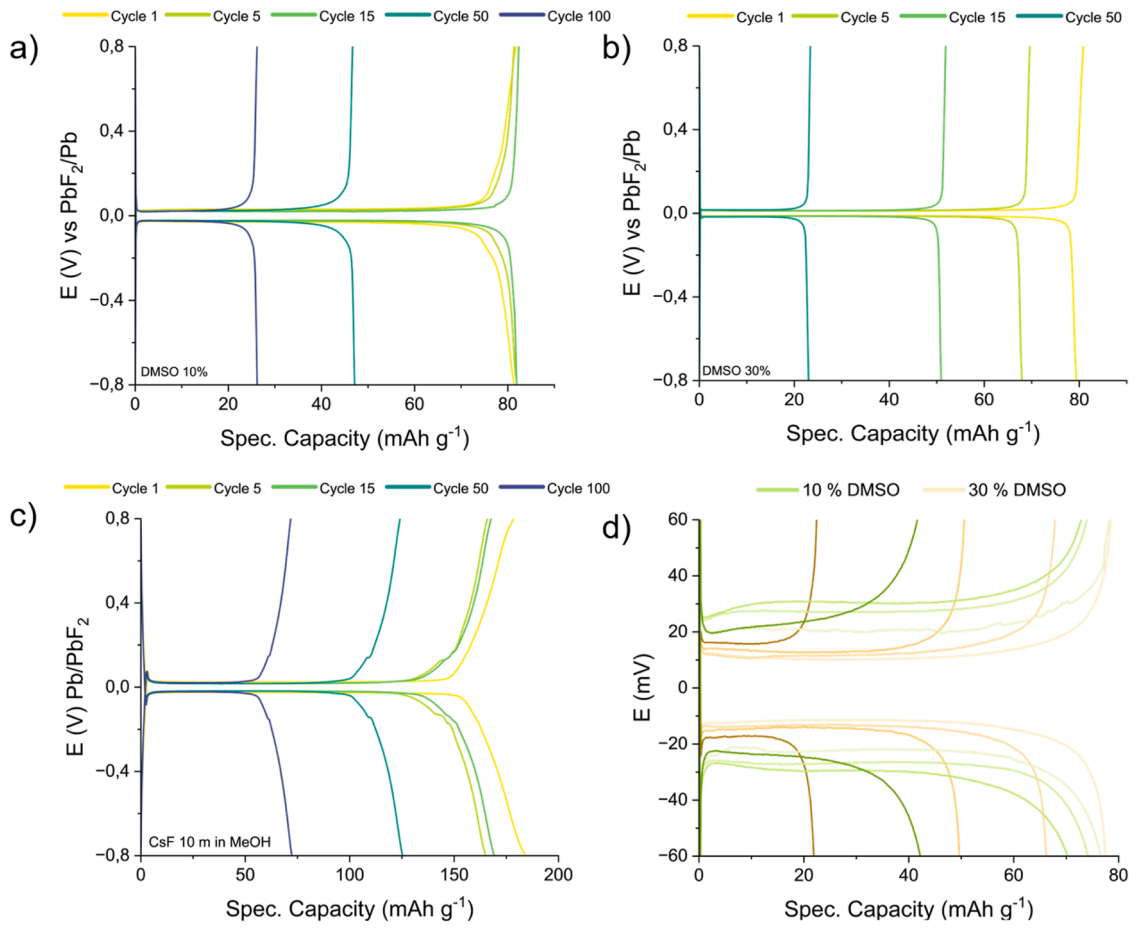


Fig. 6. Galvanostatic cycling profiles of PbF_2/Pb electrodes using a polymer electrolyte with (a) 10% DMSO and (b) 30% DMSO coelectrolytes, and (c) benchmark with CsF 10 m solution in methanol. (d) Magnification of the plateau zones of galvanostatic cycling.

corresponded to a greater degree of membrane swelling, showing a trend consistent with the ionic conductivities measured at room temperatures. While the membrane remained nearly unswollen in pure DOL, the addition of DMSO promoted solvent permeation into the polymer electrolyte matrix: a 69% mass increase was observed with 10% DMSO, whereas a value of >100% was observed with 30% DMSO (precisely +119%).

Using the Arrhenius plot, the values of σ_0 and E_a were determined for FEMs that had been swollen with different mixtures of DMSO and DOL (Fig. 5b). The addition of DMSO to pure DOL increased the ionic mobility, solvation and membrane swelling: the addition of 10% DMSO increased σ_0 by two orders of magnitude, and a further increase in the DMSO content to 30% decreased the activation energy, making the system less temperature dependent and shifting the high ionic conductivity to a higher temperature range.

The FEMs were also evaluated through galvanostatic charge-discharge cycling in a symmetric setup employing two Pb/PbF_2 electrodes as both working and counter electrodes (Fig. 6). PbF_2, with a theoretical specific capacity of 219 mAh g^{-1}, served as the capacity-limiting material. Fluorination-defluorination processes occurred during charge-discharge cycling, which was conducted at room temperature in a thermostatic chamber. The applied current was 0.1 C, corresponding to 22 mA g^{-1} relative to Pb_{F2}. For benchmarking purposes, CsF 10 m in methanol was selected because of its relatively high electrochemical stability window and ionic conductivity ($\approx 10^{-3}$ S cm^{-1}), which was suitable for cycling of Pb/PbF_2 near its theoretical specific capacity (Fig. 6c). Using different batches of the membrane and following the same electrochemical protocol, qualitatively similar galvanostatic cycling profiles were obtained (Figure S11), indicating a reproducible electrochemical response. Quantitative differences were observed between the batches, with initial specific capacities ranging approximately from 80 to 120 mAh g^{-1} and cycles from 5 to 30. These results suggested that at this stage of the research membrane and cathode preparation still influence the absolute performance. For this reason, the electrochemical results discussed below were referred to FIB assembled with membranes and electrodes prepared from the same batch. Under these conditions, all the cells were cycled for >50 cycles, with the 10% DMSO solution achieving up to 100 cycles. The initial capacity was found to be independent of the swelling agent in the FEMs, measuring 81 mAh g^{-1} for the 10% DMSO mixture and 79 mAh g^{-1} for the 30% DMSO mixture. These values were, however, lower than the capacity obtained using the same electrodes with a CsF 10 m/methanol liquid electrolyte, which reached 184 mAh g^{-1}, close to values already observed for similar electrodes with liquid electrolytes [12,41] This discrepancy may arise from the poorer interfacial contact between the electrode and the QSPE compared with the liquid electrolyte. The galvanostatic cycling results confirmed a correlation between electrolyte composition and cycling stability. The 30% DMSO mixture exhibited significant capacity fading, with a 71% loss after 50 cycles, despite the lower charge-discharge hysteresis (27 mV, compared with 52 mV for the 10% DMSO electrolyte) due to its higher ionic conductivity (Fig. 6d). In contrast, the 10% DMSO electrolyte retained 58% of its initial capacity, which was closer to the value of 68% observed with the liquid electrolyte. This difference in capacity retention can be attributed to the lower electrochemical stability of the 30% DMSO mixture, as indicated by the average coulombic efficiency during galvanostatic cycling (98.9% for 10% DMSO and 95.3% for 30% DMSO) and by LSV measurements (Figure S12). The latter showed a wide electrochemical window of 3.6 V with a less positive cathodic limit

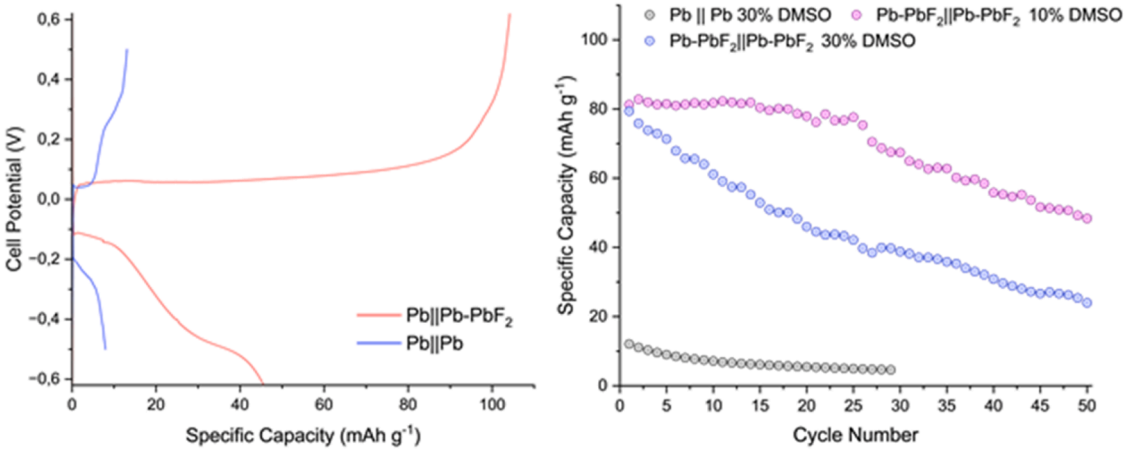


Fig. 7. Comparison between galvanostatic cycling profiles of first cycle of PbF_2 || Pb-PbF_2 and Pb||Pb cells (a) and Pb || Pb (b) and Pb-PbF_2 || Pb-PbF_2 capacity per cycle in coin-cell setup using polymer electrolyte membrane and 30% DMSO as swelling agent.

of +1.5 V vs. Ag^+/Ag, compared with +2.0 V vs. Ag^+/Ag for the 10% DMSO solution. Additionally, due to its higher polarity the higher DMSO content can increase the solubility of PbF_2 leading to an active material loss, as already observed in other lead-based FIBs systems with polar solvents [12,42] These findings suggest that although a higher DMSO content enhances the ionic conductivity and solvent uptake, excess free DMSO negatively affects the long-term stability.

Finally, a symmetrical cell with Pb || Pb electrodes was also assembled to confirm that the observed specific capacity was originated by fluorination/defluorination reactions due to F^- shuttling mechanism, rather than by plating/stripping of Pb at the electrodes (Fig. 7). A reversible capacity lower than 13 mAh g^{-1} was measured, which can be attributed to electrolyte degradation processes, presence of moisture and traces of other anions, such as OH^- [16] These anions can be exchanged through the anionic membrane and could be likely present in Pb electrodes, as $Pb(OH)_2$ formed by reaction of metallic Pb particles with moisture and air during electrodes synthesis and cell assembly steps.

4. Conclusions

This paper introduces the first fluoride-exchange membrane (FEM) based on a tetraalkylammonium-functionalized perfluorosulfonic amide ionomer as a quasi-solid polymer electrolyte (QSPE) for fluoride-ion batteries (FIBs) operating at room temperature. According to a comprehensive combination of experimental characterization and molecular dynamics simulations, the FEM showed a fluoride-ion conductivity of up to 10^{-3} S cm^{-1} when swollen with an optimized DMSO:DOL solvent mixture. MD simulations revealed that DMSO plays a fundamental role in promoting membrane swelling, thus enhancing chain extension, cavity formation and exposure of ionic moieties, which improves the ionic conductivity. Electrochemical testing confirmed that reversible fluorination/defluorination processes occurred over 50 cycles, with an initial specific capacity of approximately 80 mAh g^{-1}. These findings demonstrate the practical potential of this novel FEM for room-temperature FIBs, marking a significant advance toward the development of future scalable and commercially viable fluoride-ion energy storage systems.

CRediT authorship contribution statement

Federico Maria Scesa: Writing – original draft, Methodology, Investigation, Data curation, Conceptualization. **Maurizio Sansotera:** Writing – review & editing, Validation, Supervision, Resources, Conceptualization. **Eugenio Gibertini:** Validation, Formal analysis, Data curation. **Sinan Baris Uncu:** Investigation, Formal analysis. **Marco Gregorio:** Investigation, Data curation. **Giuseppina Raffaini:** Writing – original draft, Software, Methodology, Formal analysis, Data curation. **Luca Magagnin:** Writing – review & editing, Resources, Project administration, Funding acquisition.

Declaration of competing interest

The authors declare that they have no known competing financial interests or personal relationships that could have appeared to influence the work reported in this paper.

Supplementary materials

Supplementary material associated with this article can be found, in the online version, at doi:10.1016/j.ensm.2026.105410.

Data availability

Data will be made available on request.

References

[1] A.W. Xiao, G. Galatolo, M. Pasta, Joule 5 (2021) 2823–2844.
[2] M.A. Nowroozi, I. Mohammad, P. Molaiyan, K. Wissel, A.R. Munnangi, O. Clemens, J. Mater. Chem. A 9 (2021) 5980–6012.
[3] M.A. Reddy, M. Fichtner, J. Mater. Chem. 21 (2011) 17059.
[4] C.-H. Chen, C.-T. Yu, Y.-F. Chang, Int. J. Eng. Technol. Innov. 14 (2024) 244–253.
[5] A. Düvel, J. Bednarcik, V. Šepelák, P. Heitjans, J. Phys. Chem. C 118 (2014) 7117–7129.
[6] H. Chen, T. Aalto, V. Vanita, O. Clemens, Small. Struct. 5 (2024) 2300570.
[7] C. Rongeat, M. Anji Reddy, R. Witter, M. Fichtner, ACS. Appl. Mater. Interfaces. 6 (2014) 2103–2110.
[8] H. Konishi, T. Minato, T. Abe, Z. Ogumi, ChemistrySelect 5 (2020) 4943–4946.
[9] A.C. Kucuk, T. Yamanaka, T. Minato, T. Abe, J. Electrochem. Soc. 167 (2020) 120508.
[10] A. Celik Kucuk, T. Yamanaka, T. Abe, J. Mater. Chem. A 8 (2020) 22134–22142.
[11] A. Celik Kucuk, T. Abe, J. Fluor. Chem. 240 (2020) 109672.
[12] G. Galatolo, O. Alshangiti, C. Di Mino, G. Matthews, A.W. Xiao, G.J. Rees, M. Schart, Y.A. Chart, L.F. Olbrich, M. Pasta, ACS. Energy Lett. 9 (2024) 85–92.
[13] O. Alshangiti, G. Galatolo, G.J. Rees, H. Guo, J.A. Quirk, J.A. Dawson, M. Pasta, ACS. Energy Lett. 8 (2023) 2668–2673.
[14] H. Konishi, T. Minato, T. Abe, Z. Ogumi, Chem. Lett. 47 (2018) 1346–1349.
[15] V.K. Davis, C.M. Bates, K. Omichi, B.M. Savoie, N. Momčilović, Q. Xu, W.J. Wolf, M.A. Webb, K.J. Billings, N.H. Chou, S. Alayoglu, R.K. McKenney, I.M. Darolles, N. G. Nair, A. Hightower, D. Rosenberg, M. Ahmed, C.J. Brooks, T.F. Miller, R. H. Grubbs, S.C. Jones, Science 362 (2018) 1144–1148.
[16] F. Gschwind, Z. Zao-Karger, M. Fichtner, J. Mater. Chem. A 2 (2014) 1214–1218.
[17] Y. Yu, G. Li, C. Li, Adv. Funct. Mater. 35 (2025) 2410891.
[18] K. Takahashi, A. Yokoo, Y. Kaneko, T. Abe, S. Seki, Electrochemistry (2020) 20–00062.
[19] B. Motealleh, Z. Liu, R.I. Masel, J.P. Sculley, Z.R. Ni, L. Meroueh, Int. J. Hydrogen. Energy 46 (2021) 3379–3386.

[20] P. Stilli, S. Bonizzoni, F. Lohmann-Richters, L. Beverina, A. Papagni, P. Mustarelli, Electrochim. Acta 405 (2022) 139834.
[21] S. Bonizzoni, P. Stilli, F. Lohmann-Richters, C. Oldani, C. Ferrara, A. Papagni, L. Beverina, P. Mustarelli, ChemElectroChem 8 (2021) 2231–2237.
[22] S. Lee, H. Lee, T.-H. Yang, B. Bae, N.A.T. Tran, Y. Cho, N. Jung, D. Shin, Membranes 10 (2020) 306.
[23] S.S. Zhang, Batteries 9 (2023) 466.
[24] W.C. West, M.C. Smart, E.J. Brandon, L.D. Whitcanack, G.A. Plett, J. Electrochem. Soc. 155 (2008) A716.
[25] C. Pang, F. Ding, W. Sun, J. Liu, M. Hao, Y. Wang, X. Liu, Q. Xu, Electrochim. Acta 174 (2015) 230–237.
[26] G. Raffaini, S. Elli, F. Ganazzoli, J. Biomed. Mater. Res. 77A (2006) 618–626.
[27] F. Lazzari, A. Manfredi, J. Alongi, F. Ganazzoli, F. Vasile, G. Raffaini, P. Ferruti, E. Ranucci, Polymers 12 (2020) 881.
[28] S. Kage, K. Kudo, N. Nishida, H. Ikeda, N. Yoshioka, N. Ikeda, Forensic Toxicol. 26 (2008) 23–26.
[29] A.C. Lazanas, M.I. Prodromidis, ACS. Meas. Sci. Au 3 (2023) 162–193.
[30] Materials Studio 7.0 BIOVIA, Discovery Studio 2020 BIOVIA, Accelerys Inc, San Diego, CA, USA, 2000. InsightII 2000, https://www.accelrys.com.
[31] M.-J. Hwang, X. Ni, M. Waldman, C.S. Ewig, A.T. Hagler, Biopolymers 45 (1998) 435–468.
[32] W. Navarrini, B. Scrosati, S. Panero, A. Ghielmi, A. Sanguineti, G. Geniram, J. Power. Sources. 178 (2008) 783–788.
[33] M. Nishida, A. Eisenberg, Macromolecules 29 (1996) 1507–1515.
[34] A. Eisenberg, H.L. Yeager, Eds, Perfluorinated Ionomer Membranes, 180, American Chemical Society, Washington, D. C., 1982, p. 1.
[35] K.A. Mauritz, R.B. Moore, Chem. Rev. 104 (2004) 4535–4586.
[36] A. Ghielmi, P. Vaccarono, C. Troglia, V. Arcella, J. Power. Sources. 145 (2005) 108–115.
[37] L. Han, M. Yuan, H. Xie, G. Peng, Y. Xu, X. Zhang, Z. Ci, Z. Jin, Angew. Chem., Int. Ed. 64 (2025) e202425385.
[38] J.A. Elliott, S. Hanna, A.M.S. Elliott, G.E. Cooley, Polymer 42 (2001) 2251–2253.
[39] O. Alshangiti, G. Galatolo, C. Di Mino, T.F. Headen, J. Christianson, S. Merotto, G. J. Rees, Y. Delavoux, M. Swadźba-Kwaśny, M. Pasta, ACS. Energy Lett. 9 (2024) 6104–6108.
[40] V.K. Davis, S. Munoz, J. Kim, C.M. Bates, N. Momčilović, K.J. Billings, T.F. Miller, R.H. Grubbs, S.C. Jones, Mater. Chem. Front. 3 (2019) 2721–2727.
[41] H. Konishi, T. Minato, T. Abe, Z. Ogumi, J. Electroanal. Chem. 826 (2018) 60–64.
[42] Z. Fu, X. Yang, Y. Tian, X. Hu, Y. Wang, L. Lin, F. Kang, G. Wang, B. Li, D. Zhou, Energy Storage Mater. 70 (2024) 103533.